Paper No. 676

SYNTHESIS AND APPLICATIONS OF TiO_2 NANOPARTICLES

Dr. A. Ahmad, Gul Hameed Awan, Salman Aziz

SYNTHESIS AND APPLICATIONS OF TiO_2 NANOPARTICLES

Dr. A. Ahmad[1], Gul Hameed Awan[1], Salman Aziz[1]

ABSTRACT

Nanocrystalline semiconductor metal oxides have achieved a great importance in our industrial world today. They may be defined as metal oxides with crystal size between 1 and 100 nm. TiO_2 nanosize particles have attracted significant interest of materials scientists and physicists due to their special properties and have attained a great importance in several technological applications such as photocatalysis, sensors, solar cells and memory devices.

TiO_2 nanoparticles can be produced by a variety of techniques ranging from simple chemical to mechanical to vacuum methods, including many variants of physical and chemical vapor deposition techniques. In the present research work we report the synthesis of TiO_2 nanoparticles by Sol-Gel technique. The characterization of particles was carried out by XRD, TEM and XPS techniques. The importance and applications of these nanoparticles are discussed in detail.

[1] Department of Metallurgical and Materials Engineering University of Engineering and Technology, Lahore.

INTRODUCTION

Nanocrystalline semiconductor TiO_2 particles are of interest due to their unique properties and several potential technological applications such as photocatalysis, sensors, solar cells and memory devices (1-4). TiO_2 exists in three polymorphic phases: rutile (tetragonal density = 4.25 g/cm^3), anatase (tetragonal, 3.894 g/cm^3) and brookite(orthorhombic, 4.12 g/cm^3). Both anatase and rutile have tetragonal crystal structures but belong to different space groups. Anatase has the space group $I4_1/amd$ (4) with four formula units in one unit cell and rutile has the space group $P4_2/mnm$ (5) with two TiO_2 formula units in one unit cell (5,6). The low-density solid phases are less stable and undergo transition rutile in the solid state. The transformation is accelerated by heat treatment and occurs at temperatures between 450 and 1200^{o}C (7). This transformation is dependent on several parameters such as initial particle size, initial phase, dopant concentration, reaction atmosphere and annealing temperature, etc. (8-11).

Crystal Structure of TiO_2

Among the three above mentioned crystal structures of TiO_2, anatase owing to its higher photocatalytic activity is commonly used for photocatalysis (12). This higher photocatalytic activity is related to its lattice structure. Each Ti atom is coordinated to six oxygen atoms in anatase tetragonal unit cell. Yong et.el. (12) have reported a significant degree of buckling associated with O-Ti-O bonds in anatase compared to rutile TiO_2. Crystal symmetry is reduced due to this buckling and in turn it results a larger unit cell dimensions in the (001) direction. The kinetics of phase transformations in TiO_2 is extensively reviewed by Zhang & Banfield et al (6, 8, 9). Fig.1 shows the unit cell structures of the anatase and rutile crystals. The titanium and oxygen atoms are more tightly packed in the rutile crystal. Both structures can be described in terms of chains of TiO_2 octahedra. Each Ti^{+4} ion is surrounded by an octahedron of six O^{-2} ions. The octahedron in rutile is not regular, showing a slight orthorhombic distortion. The octahedron in anatase is significantly distorted so that its symmetry is lower than orthorhombic. The Ti-Ti distance in anatase is greater whereas the Ti-O distances are shorter than in rutile. In the rutile structures each octahedron is in contact with 10 neighbor octahedrons (two sharing edge oxygen pairs and eight sharing corner oxygen atoms) while in the anatase structure each octahedron is in contact with eight neighbors (four sharing an edge and four sharing a corner). These differences in lattice structures cause different mass densities and electronic band structures between the two forms of TiO_2 as indicated in Fig.1. Anatase can be conceived as an arrangement of parallel octahedral, while in case of rutile some octahedral are rotated by 90^o. There is a symmetry change from $I4_1/amd$ to $P4_2/mnm$ space group in terms of reconstructive polymorphism during conversion from anatase to rutile. As a consequence, the ionic mobility that occurs during phase transition results in increased densification and coarsening of the TiO_2 nanoparticles (6, 8, 9).

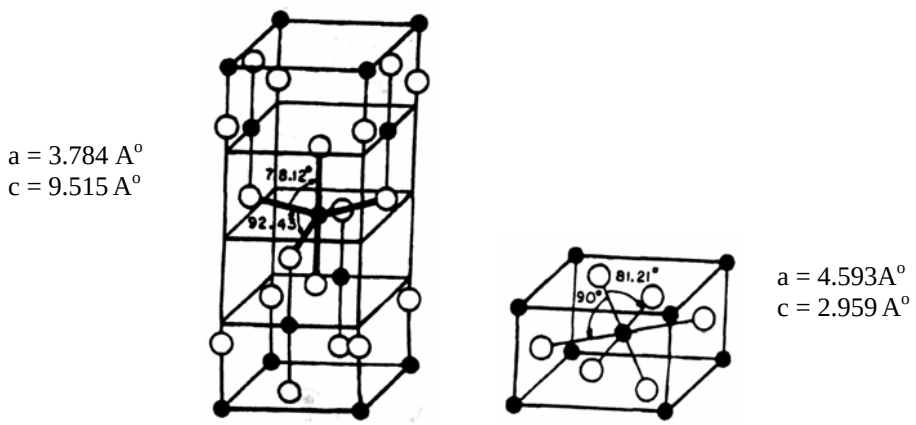

Fig. 1 Structure of anatase and Rutile TiO_2 (a) anatase (b) rutile

TiO_2 is stable in aqueous media and is tolerant of both acidic and alkaline solutions. It is inexpensive, recyclable, reusable and relatively simple to produce. It can also be synthesized in nanostructure forms more readily than many other catalysts. Furthermore, its bandgap is appropriate to initiate a variety of organic reactions.

Semiconductor photocatalysis uses sunlight to activate nanoparticles catalysts to break down these chemicals. Photocatalysis works on the principle that light falling on a semiconductor with an appropriate bandgap, or energy difference between the conduction and the valance bands will create positive (holes) and negative (electrons) charge carriers, which can in turn be used to initiate reduction (electrons) and oxidation (holes) reactions at the catalyst surface. Several competing effects inherently limit catalyst efficiency. The positively charged holes and negatively charged electrons tend, by nature, to recombine to yield a neutral state, through reemission of a photon (light) or a phonon (heat). This can occur via volumetric and surface recombination. Nanostructured (~20-30nm) particles provide the optimal balance between these effects and are thus best suited to photocatalysis. An additional advantage obtained in nanoparticles in the few tens of nm size regime is that the large surface /volume ratio makes possible the timely utilization of photogenerated carriers in interfacial processes (4,5).

TiO_2 nanoparticles can be synthesized using various methods such as sulfate process (13), chloride process (13), impregnation (14), coprecipitation (15), hydrothermal method (16-18), direct oxidation of $TiCl_4$ (19), metal organic chemical vapor deposition method, etc.(1, 20). Sol-gel method (21-23) is one of the most convenient ways to synthesize various metal oxides due to low cost, ease of fabrication and low processing temperatures. It is widely used to prepare TiO_2 for films, particles or monoliths. In general, the sol gel process involves the transition of a system from a liquid “sol” (mostly colloidal) into a solid “gel” phase. The homogeneity of the gels depends on the solubility of reagents in the solvent, the sequence of addition of reactants, the temperature and the pH. The precursors normally used for the synthesis and doping of nanoparticles are organic alkoxides,

acetates or acetylacetonates as well as inorganic salts such as chlorides. Among the classes of solvents, alcohols are largely used but other solvents such as benzene may also be used for some alkoxides.

Experimental

The titania nanoparticles were synthesized by drop wise addition of titanium tetrachloride: $TiCl_4$ (Fluka 98%) in ethanol (Pharmco 200 proof). The reaction was performed at room temperature while stirring under a fume hood due to the large amount of Cl_2 and HCl gases evolved in this reaction. The resulting yellow solution was allowed to rest and cool back to room temperature as the gas evolution ceased. The suspensions obtained were dried in an oven for several hours at 80 ^oC until amorphous and dried TiO_2 particles were obtained. The obtained powder samples were calcined for one hour in a box furnace at temperature ranging from 300 to 850 ^oC in an ambient atmosphere. To study the time dependence of phase transformation and particle growth rate, samples were also calcined by varying calcinations time for 0.5 to 2 hours. XRD patterns were recorded on as prepared and calcined samples using a Rigaku D-Max B diffractometer equipped with a graphite crystal monochromator, operating with a Cu anode and a sealed X-ray tube. The 2Θ scans were recorded at several resolutions using Cu K_α radiation of wavelength 1.54 Å in the range 20-80^o with 0.05^o step size. The recorded patterns were analyzed using Jade® software to determine peak position, width and intensity. Full-width at half-maxima (FWHM) data was analyzed by Scherer's formula (equation No.1) to determine average particle size. Scherer's equation is given by

$$t = \frac{0.9\lambda}{\beta Cos\theta} \qquad \text{(eq.1)}$$

where λ is the X-ray wavelength, β is the peak width and theta is the Bragg's angle. Since peak width used in the Scherer's formula also includes the line broadening due to strain in the particles, measurements of particle size and distribution were also carried out by TEM. Both bright field and dark field micrographs were taken with a JEOL JEM-2000FX operating at 200 kV. Samples for TEM were prepared by dropping a dilute suspension of the sample powders onto a 300-mesh Lacy carbon grid. Dilute suspension was prepared by sonicating the particles in acetone for 5 to 10 minutes.

The lattice constants of calcined samples was also measured. For this analysis only samples containing the anatase phase were used, to avoid the effect of rutile crystals segregated out of anatase system. Samples were annealed at 500 ^oC for 1 hour before analysis for XRD. The peak positions (2θ) of the anatase (101) and (200) reflections were used to calculate the lattice parameters using the following formula (equation 2)

$$d = \frac{1}{(h/a + k/a + l/c)^{1/2}} \qquad \text{(eq.2)}$$

The value of d, for an XRD peak can be determined from the 2θ angle by Bragg's Law (Eq.3)

$$d = \frac{\lambda}{2\sin\theta} \qquad \text{(eq.3)}$$

where λ is the X-ray wavelength and θ is in radians.

The mass fraction of rutile (X_r) in the samples calcined at various temperatures was calculated based on the relationship between the integrated intensities of anatase (101) and rutile (110) peaks by the following formula developed by Spurr and Myers

$$\mathrm{Xr} = \frac{1}{(1 + KI_a / I_r)} \qquad \text{(eq. 4)}$$

where I_a and I_r are the integrated peak intensities of anatase and rutile peaks respectively. The constant K was determined previously by A. Burns et al (16) and Barakat et al (20) via an XRD analysis of standard mixture of TiO_2 powder (Degussa P-25) of known proportions of anatase and rutile (80:20) and is equal to 0.79.

The activation energy, E_a for the anatase to rutile phase transformation were calculated from the slope of the plot of the corrected rutile weight fractions, Xr as a function of the reciprocal of annealing temperature from XRD spectra. The relationship is given as below:

$$\ln X_r = -\frac{E_a}{R}\frac{1}{T} \qquad \text{(eq. 5)}$$

$$E_a = -\frac{\partial \ln(Xr)}{\partial(1/T)}\frac{R}{1000} \qquad \text{(eq. 6)}$$

where E_a is the anatase to rutile transformation activation energy, T is temperature in Kelvin, R is the universal gas constant (8.314 J/mol K) and X_r is the corrected weight fraction of rutile as defined earlier.

Results and Discussion:

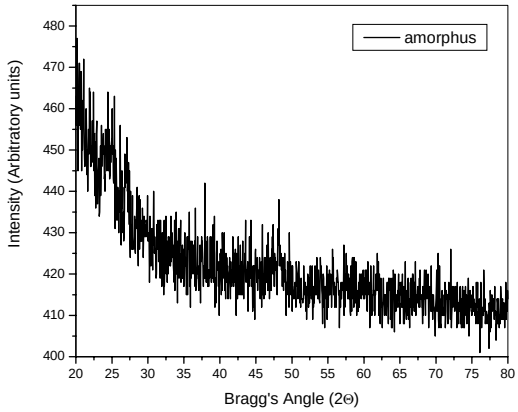

Fig 1- X-ray diffraction pattern as synthesized TiO_2 nano particles.

Fig.1 shows the X-ray diffraction pattern for as-prepared TiO_2 synthesized via so-gel route. As prepared nanosize particles showed amorphous structure. Fig.2 shows the XRD patterns of TiO_2 samples annealed at various temperatures. Annealing resulted in diffraction peaks related only to the anatase and rutile polymorphs of TiO_2. From 300 ^oC to 650 ^oC only peaks related to anatase structure were evident. Above 650 ^oC rutile peaks started to appear and a

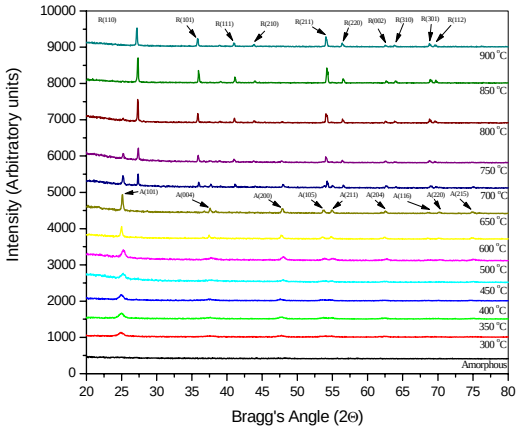

Fig 2- X-ray diffraction patterns of TiO_2 annealed at various temperatures.

mixture of both the anatase and rutile phases of TiO_2 existed up to 800 ^oC. At 850 ^oC, the XRD pattern showed a complete transformation from anatase to rutile.

From the XRD data of Fig. 2, it is evident that the crystallite size increases with increasing calcinations temperature and that the diffraction peaks become intense and their FWHM gradually became narrow suggesting an increase in particles size and increase in the amount of the pertinent phase. The anatase (101) peak was used to determine the grain size by Scherer's formula. The results of the grain size analysis is shown in Fig. 3.

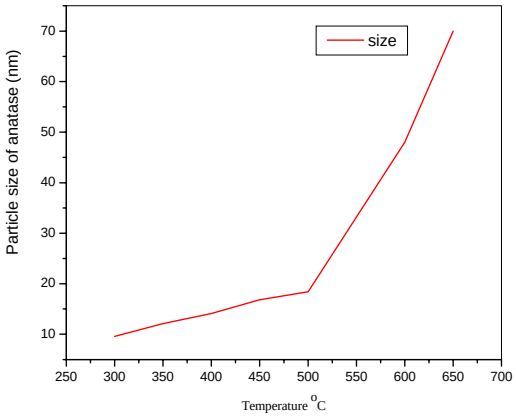

Fig 3- Variation of particles size as a function of calcination temperature.

The particle size of TiO_2 annealed at various temperatures was also analyzed by TEM. Figures 4 show the TEM bright field image, of TiO_2 at 500 ^oC for 1 hour. The particles size measured by TEM were generally in agreement with those determined by XRD though some agglomeration is present due to high surface energy of the particles.

The TiO_2 anatase unit cell is tetragonal with lattice parameters "a" and "c" corresponding to 3.78 and 9.52 Å, respectively. Rutile is also tetragonal with "a" and "c" parameters as 4.59 and 2.96 Å, respectively. The lattice constants a and c of anatase structure were determined by XRD. This analysis was performed on samples annealed at 500 ^oC for 1 hour, i.e., well below the anatase to rutile transformation temperature, in order to avoid the effects of rutile crystal precipitating out of the anatase lattice. The peak values of the anatase (101) and (200) reflections were used to calculate the lattice parameters. The lattice parameter *a* and *c* were in good agreement with the literature.

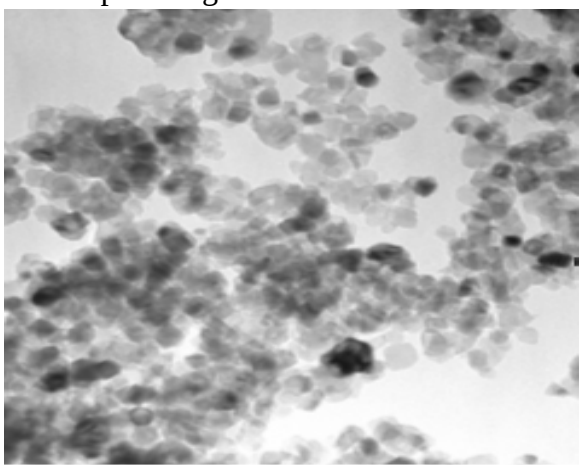

Figure 4- EM bright field image of TiO_2 annealed calcined at 500oC for one hour.

Fig.5 shows the effect of calcination temperature on the anatase to rutile phase transformation for undoped TiO_2 samples. Mass fraction of rutile phase was calculated according to the equation 3, based on the integrated intensity ratio(I_r/I_a) of rutile and anatase XRD peaks. The peaks chosen for the calculation of this ratio were (101) and (110) peaks as the anatase and rutile peaks, respectively. Tables 1 summarize the XRD results showing the percentage of phases observed for undoped samples.

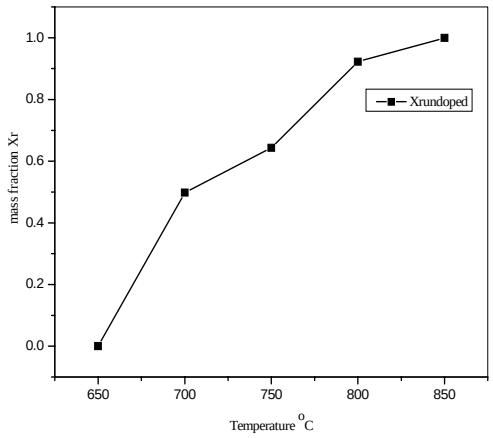

Fig 5- Effect of calcination temperature on the anatase to rutile phase transformation for TiO2 nano particles.

Temperature	Time	%Rutile	%Anatase
40 oC	48hrs	Amorphous	
300 oC	1hr	0	100
350 oC	1hr	0	100
400 oC	1hr	0	100
450 oC	1hr	0	100
500 oC	1hr	0	100
600 oC	1hr	0	100
650 oC	1hr	0	100
700 oC	1hr	24	76
750 oC	1hr	78.7	21.3
800 oC	1hr	96.9	3.1
850 oC	1hr	100	0
900 oC	1hr	100	0

Table-I: % age of Phases observed.

As expected, the percentage of rutile phase increased with the increase in calcination temperatures.

CONCLUSIONS

- As prepared TiO_2 particles are amorphous in nature.
- Amorphous to anatase transformation started at temperature above 250^{o}C.
- Anatase was stable upto temperature 650^{o}C.
- The anatase-to-rutile transformation started at temperature above 650^{o}C.
- Mass fraction of rutile was increased with the rise in calcination temperature.
- Particle size of anataze was increased as the calcination temperature was increased.

REFERENCES

1. W.Li, S.Ismat Shah, C.P Huang, O.Jung and C.Ni, Mater. Sci.Eng. B 96, 247 (2002)

2. J.T.Remillard, J.R.McBride, K.E.Nietering, A.R.Drews and X.Zhang, J.Phys.Chem.B104, 4440 (2000)
3. E.Traversa, J.Am.Ceram.Soc.78, 2625 (1995)
4. A.I.Kingon, J.P.Maris and S.K.Steiffer, Nature (London) 406, 1032 (2000)
5. W.Li, C.Ni, H.Lin, C.P.Huang and S.Ismat Shah, Journal of Applied Physics, Volume 96, No.11, 6663 (2004)
6. H.Zhang.and J.F.Banfield, Am.Mineral.84, 528 (1999)
7. A. Tsevis, N. Spanos, P. G. Koutsoukos, Ab J. Van der Linde and J. Lyklema, J. Chem.Soc, Faraday Trans; 94(2), 295 (1998)
8. H. Z. Zhang and J.F.Banfield, J.Mater.Chem. 8, 2073 (1998)
9. H.Z.Zhang and J.F.Banfield, J.Phys.Chem.B 104, 3481(2000)
10. M.R.Ranade, A.Navrotsky, H.Z.Zhang, J.F.Banfield, S.H.Elder, A.Zaban, P.H.Borse, S.K.Kulkarni, G.S.Doran and H.J.Whitfield, PNAS99, 6476 (2.11.02)
11. J.Arbiol, J.Cerda, G.Dezanneau, A.Cirera, F.Peiro, A.Cornet and J.R.Mornate, J.Apply.Phy.92, 853 (2002)
12. Yong Liang, Shupan Gan, Scott A.Chambers and Eric I.Altman, Physical Review B, Vol. 63, 235402-1 (2001)
13. M. Howe.Grant (Ed), Kirk-Othmer Encyclopedia of Chemical Technology, vol.24, John Wiley & Sons, Inc, p.225, 1997
14. M.I.Litter, J.A.Navio, J.Photochem.Photobiol.A.Chem.84 183, (1994)
15. L.Palmisano, V.Augugliaro, A.Sclafani. M.Schiavello.J.Phys.Chem.92, 6710 (1988)
16. Y.Wang.H.Cheng.Y.Hao.J.Ma. W. Li. S.Cai, J. Mater.Sci 34, 3721(1999)
17. H. Cheng. J.Ma, Z.Zhao, L.Qi, Chem.Mater. 7, 663 (1995)
18. Y.Wang, Y.Hao, H.Cheng, J.Ma, B. Xu, W. Li, S. Cai, J. Mater. Sci. 34, 2773 (1999)
19. M.K.Akhtar, Y.Xiong, S.E.Pratsinis, AIChE J.37, 1561(1991)
20. Z.Ding, X.Hu.G.Q.Lu, P.L.Yue, P.F.Greenfield, Langmuir 166216 (2000)
21. C.C.Wang, Z.Zhang, J.Y.Ying, NanoStructured Mater. 9, 583 (1997)
22. A.Burns, W.Li, C. Baker, S.I.Shah, Mater. Res. Soc. Symp. Proc.V.5.2.703 (2002)
23. Andrew Burns, G.Hayes, W.Li, J.Hirvonen, J.Derek Demaree, S.Ismat Shah, Materials Science and Engineering, BXXX MSB 9793 1-6 (2004)
24. F.M.F.de Groot and J.C.Fuggle, Physics Review B vol 41 No.2, 928(1990)